Preparation and characterization of low-amount Yb^{3+}-doped TiO_2 photocatalyst

H. Q. Jiang,[a,b] P. Wang,[a]★ X. L. Guo,[a] and H. Z. Xian[a]

[a]*Research Center for Green Chemical Technology, School of Municipal and Environmental Engineering, Harbin Institute of Technology, Harbin 150090, China. Fax: 86 (451) 8260 3898. E-mail: pwang73@hit.edu.cn*

[b]*Department of Chemistry, Harbin Normal University, Harbin 150500, China. E-mail: h.q.jiang1119@163.com*

The nanoparticles of Yb^{3+}-doped (0.125 wt.%) and pure TiO_2 were prepared by an acid-catalyzed sol-gel method and characterized by X-ray diffraction, X-ray photoelectron spectroscopy, UV—Vis diffuse reflectance spectroscopy, and surface photovoltage spectroscopy; the specific surface of the samples was measured using the Brunauer—Emmett—Teller (BET) method. The photocatalytic degradation of methylene blue in aqueous solution was used as a probe reaction to estimate the photocatalytic activity of the prepared nanoparticles. The photocatalytic activity of Yb^{3+}/TiO_2 composite nanoparticles is much higher than that of pure TiO_2. A low amount of Yb^{3+} in TiO_2 can inhibit the anatase—rutile phase transformation of TiO_2, prevent grain growth increasing the specific surface area, and favor the high-temperature stabilization of the pores. According to the surface voltage spectroscopy data, Tb^{3+}-doping prevents recombination of photoinduced electrons and holes and improves the light absorption capacity of the particle surface.

Key words: titania, Yb^{3+}-doping, nanopowders, photocatalytic activity.

Heterogeneous photocatalysis for the environmental-friendly technology has attracted considerable attention due to its great potential of application in water and air purification in recent years. Among various semiconducting photocatalysts, nanocrystalline TiO_2 is believed to be one of the most promising photocatalytic materials due to its strong oxidizing power, chemical stability, non-toxicity, photocorrosion resistance, cheapness, and commercial availability.[1—3] However, two drawbacks, a wide band gap and a high recombination rate of photogenerated electron-hole pairs resulting in a low quantum efficiency, hamper to a great extent its commercial applications in the technology of environmental purification.[4,5]

The photocatalytic activity of nanocrystalline TiO_2 can be enhanced by the introduction of foreign metal ions.[6—10] Researchers have shown[9,10] that doping of nanocrystalline TiO_2 with rare-earth ions can enhance the photocatalytic activity, while the nature and amount of doping ions can significantly affect the recombination rate of photogenerated electron-hole pairs at the surface and in the crystalline lattice of the catalyst and the interfacial charge-transfer efficiency. Our preliminary experiments showed that the Yb^{3+} content and calcination temperature influenced the photocatalytic activity of the Yb^{3+}-doped TiO_2 nanoparticles and Yb^{3+}-doping could improve the photocatalytic activity of the sample. Surprisingly, the prepared composite nanoparticles containing 0.125 wt.% Yb^{3+} (*i.e.*, much lower than the optimal doping content reported in literature[10]) exhibited the highest photocatalytic activity among the Yb^{3+}-doped samples. The mechanism of effect of low amounts of Yb^{3+} on the photocatalytic activity of TiO_2 has not been well understood.

The task of the present article is to reveal the mechanism of effect of Yb^{3+}-doping, prepare pure and Yb^{3+}-doped (0.125 wt.%) TiO_2 nanoparticles by the acid-catalyzed sol-gel method, and study the effect of low-amount Yb^{3+}-doping on the phase structure, crystallite size, surface texture properties, surface chemical composition, light absorption capacity, and surface photovoltaic properties of the nanoparticles. The photocatalytic degradation of the methylene blue dye in aqueous solution was used as a probe reaction to estimate the photocatalytic activity of the prepared nanoparticles.

Experimental

Pure and Yb^{3+}-doped titania nanoparticles were prepared by the acid-catalyzed sol-gel technique using $Ti(OBu)_4$ and $Yb(NO_3)_3$ as precursors. To obtain transparent solution *A*, $Ti(OBu)_4$ (20 mL) was added dropwise to anhydrous EtOH (60 mL) under continuous stirring for 20 min. Transparent solu-

Published in Russian in *Izvestiya Akademii Nauk. Seriya Khimicheskaya,* No. 10, pp. 1680—1685, October, 2006.

1066-5285/06/5510-1743

tion *B* containing of anhydrous EtOH (20 mL), distilled water (10 mL), concentrated HNO_3 (1.5 mL), and a specified amount of ytterbium nitrate was slowly added to solution *A* under vigorous stirring for 1 h at room temperature to give a light yellow transparent sol. The gel was prepared by aging the sol for several days at room temperature. The gel was dried at 80 °C for 12 h to remove the solvents and then calcined in air at 600 °C for 2 h and then milled into powder to obtain Yb^{3+}-doped TiO_2 composite nanoparticles. Pure TiO_2 was prepared by the same procedure without addition of dopant.

The crystallite structures of the photocatalysts were studied by X-ray diffraction on a Japan Shimadzu XRD-6000 X-ray diffractometer (Cu-Kα radiation, λ = 0.15418 nm, nickel filter). The measurements were carried out at a tube voltage of 30 kV and a current of 30 mA.

The BET surface area pore volume and average pore size of the catalysts were analyzed by N_2 adsorption—desorption method using an AUTOSORB-1 apparatus (Quantachrome Instruments Inc.) at 77 K. Before measurement, the samples were evacuated at 423 K for 3 h.

The surface elemental composition and chemical states of the samples were examined by X-ray photoelectron spectroscopy with a PHI5700 instrument using a monochromatic aluminum X-ray source. The binding energies were calibrated with respect to the signal for carbon (binding energy 248.6 eV) that is present in the chamber as impurity hydrocarbons.

The diffuse reflectance spectra of the samples were recorded with a PE Lambda900 UV—Vis—NIR spectrometer equipped with an integrating sphere at room temperature in air in a range of 200—800 nm. The baseline was corrected using a calibrated sample of barium sulfate.

The surface voltage spectra of the samples were obtained with the surface photovoltage spectrometer made by the Department of Chemistry of the Jilin University[11] and equipped with a photovoltage cell mainly consisting of two ITO (In_2O_3—SnO_2)—quartz glass electrodes.

The photocatalytic decoloration of methylene blue in aqueous solution was used as probe reaction to estimate the photocatalytic activity. An aqueous solution of methylene blue ($2.8 \cdot 10^{-5}$ mol L^{-1}) was placed in a 100-mL Pyrex glass beaker, and a nanopowder (0.050 g) was added with stirring. Then the photocatalysis was started by irradiating the reaction mixture with UV light source positioned 15 cm above the solution stirred at room temperature. A 15-W lamp with a characteristic wavelength of 254 nm was used as a UV light source. After reaction for 1 h, the mixture was centrifuged for 30 min to separate the powders from the solution. The uppermost 5 mL of the dye solution were then removed with a pipette, and the absorbance was measured using a 762 UV—Vis spectrometer at a wavelength of 664 nm.

A preliminary test showed a good linear relationship between the absorbance and dye concentration in a certain concentration range. The general removal rate of methylene blue was then calculated by the substitution of the absorbance for the concentration. The removal of methylene blue resulted from both the photocatalytic decoloring and adsorptive removal of the powders. Therefore, the blank adsorption experiment should be completed under the same conditions except for illumination in parallel. The photocatalytic decoloration rate used to estimate the photocatalytic activity was calculated by subtracting the adsorptive removal rate from the general removal rate.

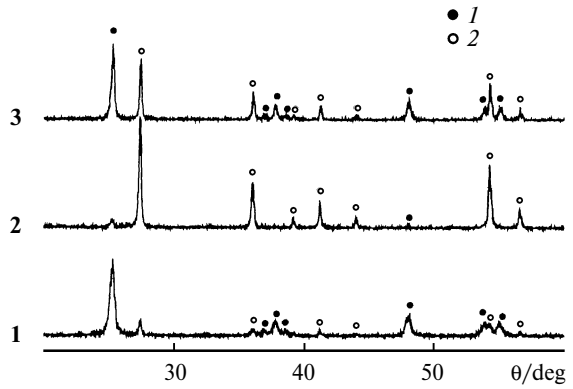

Fig. 1. X-ray powder diffraction patterns of nanoparticles of samples **1**, **2**, and **3**: *1*, anatase and *2*, rutile.

Results and Discussion

The X-ray diffraction data for pure TiO_2 nanopowders calcined at 500 (**1**) and 600 °C (**2**) and Yb^{3+}-doped TiO_2 nanopowder calcined at 600 °C (**3**) are given in Fig. 1. It can be seen from these data that the observed reflections can be attributed to anatase or rutile and there are no reflections from ytterbium oxides. A possible reason is that the amount of Yb_2O_3 was too low to be detected by X-ray diffraction analysis. The results indicate that the added Yb_2O_3 is well dispersed in the TiO_2 particles and not gathered in local position.

The anatase of TiO_2 is in metastable phase and should transform into rutile during sintering at high temperature with energy release. According to Fig. 1, nanopowders **1** contain 81% anatase but **2** contain only 7%, indicating that the phase transformation from anatase to rutile has almost been completed. However, in sample **3** the amount of anatase decreases to 56%, which shows that low-amount Yb^{3+}-doping can obviously inhibit the anatase to rutile phase transformation and enhance the temperature of the phase transformation. According to the Scherrer formula, the average crystallite sizes of the main crystal phase of nanoparticles **1**, **2**, and **3** are 20.3, 28.7, and 26.3 nm, respectively. Thus, the presence of a low amount of Yb^{3+} in TiO_2 nanoparticles can result in a decrease in its crystallite size.

The Ti^{4+} and Yb^{3+} ion radii are 68.0 and 85.9 pm, respectively. Since the Yb^{3+} ion radius is much larger than that of the Ti^{4+} ion, the Yb^{3+} ions introduced by the sol-gel process cannot enter into the lattice of the anatase phase to form a stable solid solution. During the drying and calcination with the removal of liquids and organic substances the uniformly dispersed Yb^{3+} ions will gradually migrate from the volume of anatase grains to the surface.[12] The Ti^{4+} ions at the interface can be substituted by Yb^{3+} from the Yb_2O_3 lattice to form Ti—O—Yb bonds around the anatase crystallite and form tetrahedral Ti sites.[9] The anatase—rutile phase transformation needs

Table 1. BET specific surface and pore parameters of nanoparticles **1** and **3**

Sample	Specific surface area /$m^2\ g^{-1}$	Pore volume /$cm^3\ g^{-1}$	Average pore size /nm
1	2.8	0.006	6.16
3	4.9	0.011	9.22

rutile nucleation at the surface of anatase grains.[13] Consequently, the formed Ti—O—Yb bonds and the presence of interstitial Yb_2O_3 will inhibit the anatase to rutile phase transformation and grain growth.

The BET specific surface area and pore parameters of nanopowders **1** and **3** are given in Table 1. It is obvious that the specific surface areas, pore volumes, and average pore size of nanopowders **3** exceed those for **1**. The results corroborate that low-amount Yb^{3+}-doping can markedly improve the surface texture properties of TiO_2 nanopowders and enhance the thermal stability of their microtexture. Generally speaking, calcination at high temperature can make the pores bigger while the pore volume smaller. There are two factors increasing pore sizes. First, the smaller pore endures much greater stress than the bigger pores, so the small pores collapse firstly during calcination. Second, the bigger crystallite aggregation can form bigger pores.[14] We think that the Yb_2O_3 is dispersed in the crystal lattice gap of TiO_2 and Ti—O—Yb bonds formed can produce a towing effect on the crystal boundary, which can enhance the diffuse potential barrier between crystallites, block the transfer of the crystal boundary, and restrain the grain growth effectively. Therefore, Yb^{3+}-doping is beneficial to the high-temperature stabilization of pores in the powders.

The larger is the specific surface area, the stronger is the adsorption ability. Therefore, the Yb^{3+}-doped particles have stronger adsorption ability to pollutants than pure TiO_2, which favors their higher photocatalytic activity.

The X-ray diffraction analysis was carried out to determine the chemical composition of the catalysts and the valent states of various species present therein. The X-ray diffraction data for powders **1** and **3** are shown in Fig. 2. It can be seen that the both samples, *viz.*, Yb^{3+}-doped (**3**) and pure TiO_2 (**1**) nanoparticles, exhibit similar patterns. The main elements are titanium, oxygen, and carbon. The latter comes from the contaminant hydrocarbons in the instrument. The results indicate that the binding energy of Ti2p and O1s is 458.365 and 529.615 eV, respectively, showing that Ti is in the form of Ti^{4+} (TiO_2) and oxygen is in the form of O^{2-}. The X-ray photoelectron spectroscopy of the Yb^{3+}-doped TiO_2 nanopowders cannot reveal a signal at ~185.5 eV, demonstrating that the ytterbium content at the surface of the sample is very low.

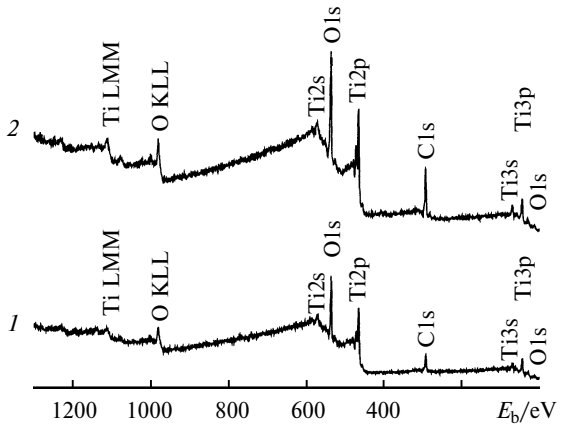

Fig. 2. X-ray photoelectron spectra of nanoparticles **1** (*1*) and **3** (*2*).

This further confirms that it is possible that the doping Yb_2O_3 is very evenly dispersed in the crystal interlacunar of TiO_2.

The O1s peak in the X-ray photoelectron spectrum (Fig. 3) is asymmetric, showing that the oxygen species on the surface of the particles contain not only the crystal lattice oxygen (529.5 eV) forming Ti—O bonds, the oxygen of the hydroxyl groups (531.5 eV) on the sample surface but also the physically adsorbed oxygen (533.0 eV). Thus, we fitted the curve the O1s peaks of the oxygen on their surface (see Fig. 3). The fitting results are listed in

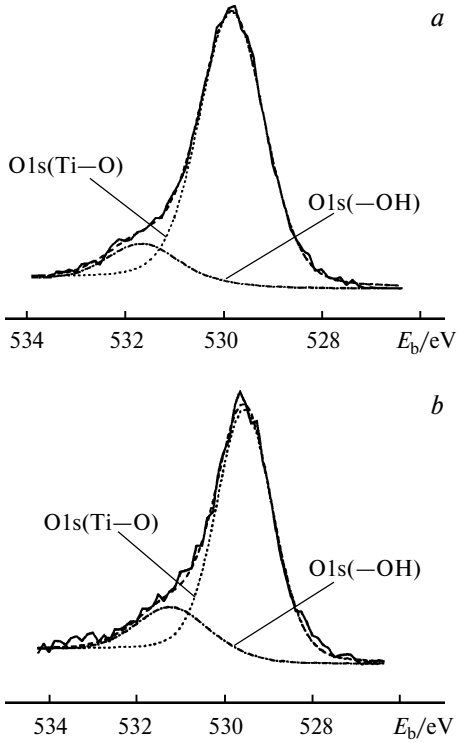

Fig. 3. X-ray photoelectron spectra in the range of the O1s peak recorded on the surface of nanoparticles **1** (*a*) and **3** (*b*).

Table 2. Curve fitting results of the X-ray photoelectron spectra for the oxygen species on the surface of nanoparticles **1** and **3**

Sample	E_b/eV (oxygen content (%))	
	O1s (Ti—O)	O1s (—OH)
1	529.81 (88.69)	531.65 (11.31)
3	529.52 (81.81)	531.20 (18.19)

Table 2. The results show that Yb^{3+}-doping can increase the content of the hydroxyl groups on the TiO_2 surface. This is partly due to the fact that the Yb^{3+}-doped TiO_2 having more abundant pores, a larger specific surface area, and a bigger pore volume, can adsorb more H_2O to form Ti—OH bonds.[15] In addition, in the TiO_2—Yb_2O_3 composite system, Ti^{4+} replaces Yb^{3+} in the Yb_2O_3 crystal lattice and creates a charge imbalance. Due to the charge imbalance, more hydroxide ions will be adsorbed on the surface for charge balance. A similar explanation has been offered for the TiO_2—La_2O_3 and TiO_2—Y_2O_3 systems.[9]

The surface hydroxyl groups play an important role in the photocatalytic oxidation of organic compounds; they are of benefit not only to the trapping of photogenerated holes to enhance the separation efficiency of electron-hole pair but also to the forming of surface free radicals ($^{\bullet}OH$) to oxidize contaminants.[15—17] At the same time, they also serve as adsorption site for organic molecules.[17] Consequently, the increase in the surface hydroxyl groups can be in favor of the enhancement in the photocatalytic activity of the sample.

The UV—Vis diffuse reflectance spectra of nanopowders **1** and **3** are shown in Fig. 4. It can be seen from these data that the reflectivity of the particles fast decreases below 427 nm, which is due to light absorption resulted from the excitation of electrons from the valence band to the conduction band of TiO_2, and the absorption edge for the doped sample shows a significant red shift. This is consistent with the results of X-ray diffraction analysis. The crystallite size of the pure sample is smaller than that of the doped sample. Therefore, a quantum size effect appears, resulting in a blue shift of the absorption edge.[18] The light absorption capability of the doped sample increases slightly, which can favor the enhancement in the photocatalytic activity.

The surface photovoltage reflects the absorption character of the sample and the recombination of light-induced electrons and holes.[11] Figure 5 shows the surface photovoltage spectra of nanopowders **1** and **3**. The positive peaks at 347 nm for sample **1** and at 350 nm for sample **3** can be attributed to the electron transition from the valence band to the conduction band.[19] The response at 413 nm for the doped sample can be assigned to the electron transition from the valence band to the conduction band of rutile, because its band gap is ~3.0 eV. The obvious tailing peak in the region of 413—600 nm can be attributed to the impurity energy level originating from Yb^{3+}-doping, because no such peak is observed for pure TiO_2 (**1**). Compared with that of pure sample **1**, the surface photovoltage spectrum of doped sample **3** shows two important features. The first one is the increased surface photovoltage response corresponding to the band-to-band transition, showing that the low amount of Yb^{3+} in TiO_2 can inhibit the recombination of photogenerated electrons and holes and enhance the separation efficiency. According to the principle of generation of surface photovoltage, for an n-type TiO_2 semiconductor, Yb^{3+}-doping results in an increase in the surface oxygen vacancies or deficiencies of TiO_2,[20] which can capture photoinduced electrons and thus efficiently restrain the recombination of electrons and holes and enhance the quantum efficiency. As a result, the surface photovoltage increases. The second feature is a broad surface photovoltage response, which indicates that the low amounts of Yb^{3+} in TiO_2 can improve the absorbability of the sample surface for visible light. These results confirm that

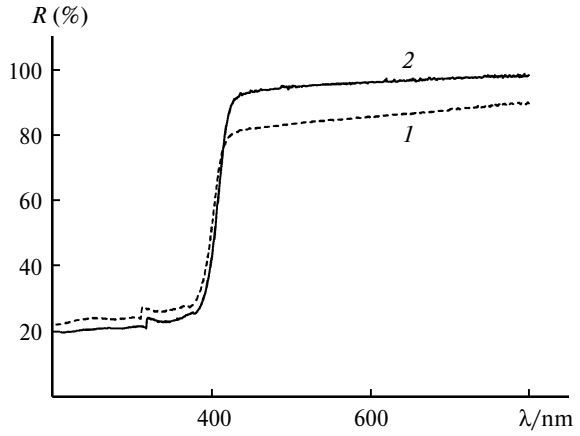

Fig. 4. UV—Vis diffuse reflectance spectra in the visible region for nanoparticles **1** (*1*) and **3** (*2*); *R* is reflectivity.

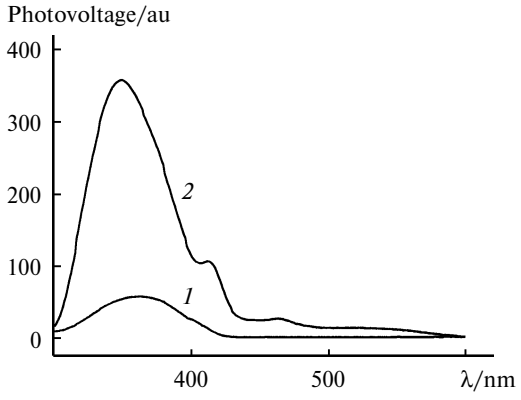

Fig. 5. Surface photovoltage spectra for nanoparticles **1** (*1*) and **3** (*2*).

Table 3. Photocatalytic acitivity of nanoparticles of pure TiO_2 and Yb^{3+}-doped TiO_2

Sample	w^a (%)	Specific photoactivity^b /mol g^{-1} h^{-1}
1	40.31	$8.01 \cdot 10^{-6}$
3	54.94	$1.03 \cdot 10^{-5}$

[a] Average degradation rate of the methylene blue dye after 1 h of the photocatalytic reaction.
[b] Methylene blue degradation amount per unit mass catalyst after 1 h of the photocatalytic reaction.

Yb^{3+}-doping can promote the separation efficiency of photogenerated electrons and holes and improve the absorbability of the sample surface for visible light, which can lead to the enhancement in the photocatalytic activity.

The photocatalytic activity values for nanopowders **1** and **3** are presented in Table 3. It is obvious that the photocatalytic activity of Yb^{3+}-doped titania (**3**) is much higher than that of the pure TiO_2 sample (**1**). According to the above analysis. we think that the enhancement in the photocatalytic activity should be ascribed to such aspects resulting from Yb^{3+}-doping as inhibiting the recombination of photogenerated electrons and holes, increasing the number of surface hydroxyl groups, enlarging the specific surface area, and improving the light absorption capability of the particle surface.

Thus, the low-amount Yb^{3+}-doped TiO_2 nanopowder with a higher photocatalytic activity has been prepared successfully by the acid-catalyzed sol-gel method. The presence of a low amount of Yb^{3+} can inhibit the phase transformation from anatase to rutile of TiO_2, suppress the grain growth, increase the specific surface area, and improve the high-temperature stabilization of pores in the composite nanopowders. Nanoparticles of Yb^{3+}-doped titania contain more surface hydroxyl groups than pure TiO_2. The absorption edge for the doped sample shows a red shift of the spectrum. The surface photovoltage spectral analysis indicates that Yb^{3+}-doping can inhibit the recombination of photogenerated electrons and holes and improve the light absorption capability of the particle surface. The enhancement in the photocatalytic activity of Yb^{3+}-doped TiO_2 nanoparticles is due to the suppression of the recombination of photoinduced electrons and holes, an increase in the number of hydroxyl groups on the surface, an enlargement of the specific surface area, and improvement of the light absorption capability of the particle surface.

The results presented can serve as a theoretical practical basis for further developments of new highly active photocatalytic ecologically safe materials appropriate for practical applications.

References

1. A. I. Kokorin, V. M. Arakelyan, and V. M. Arutyunyan, *Izv. Akad. Nauk*, *Ser. Khim.*, 2003, 88 [*Russ. Chem. Bull., Int. Ed.*, 2003, **52**, 93].
2. I. M. Arabatzis, T. Stergiopoulos, D. Andreeva, S. Kitova, S. G. Neophytides, and P. Falaras, *J. Catal.*, 2003, **220**, 127.
3. D. Li, H. Haneda, S. Hishita, N. Ohashi, and N. K. Labhsetwar, *J. Fluorine Chem.*, 2005, **126**, 69.
4. Y. Yang, X. Li, J. Chen, and L. Wang, *J. Photochem. Photobiol. A: Chem.*, 2004, **163**, 517.
5. D. Shchukin, S. Poznyak, A. Kulak, and P. Pichat, *J. Photochem. Photobiol. A: Chem.*, 2004, **162**, 423.
6. P. Yang, C. Lu, N. Hua, and Y. Du, *Mater. Lett.*, 2002, **57**, 794.
7. Y. M. Wang, S. W. Liu, M. K. Lü, S. F. Wang, F. Gu, X. Z. Gai, X. P. Cui, and J. Pan, *J. Mol. Catal. A: Chem.*, 2004, **215**, 137.
8. A. D. Paola, E. Garcia-Lopez, S. Ikeda, G. Marci, B. Ohtani, and L. Palmisano, *Catal. Today*, 2002, **75**, 87.
9. J. Lin and J. C. Yu, *J. Photochem. Photobiol. A: Chem.*, 1998, **116**, 63.
10. A. W. Xu, Y. Gao, and H. Q. Liu, *J. Catal.*, 2002, **207**, 151.
11. L. Jing, Z. Xu, X. Sun, J. Shang, and W. Cai, *Appl. Surf. Sci.*, 2001, **180**, 308.
12. H. E. Chao, Y. U. Yun, H. U. Xingfang, and A. Larbot, *J. Eur. Ceram. Soc.*, 2003, **23**, 1457.
13. B. Xia, H. Huang, and Y. Xie, *Mater. Sci. Eng. B*, 1999, **57**, 150.
14. J. Yu, M. Zhou, B. Cheng, H. Yu, and X. Zhao, *J. Mol. Catal. A: Chem.*, 2005, **227**, 75.
15. S. Liao, D. Huang, D. Yu, Y. Su, and G. Yuan, *J. Photochem. Photobiol. A: Chem.*, 2004, **168**, 7.
16. A. Mills and S. L. Hunte, *J. Photochem. Photobiol. A: Chem.*, 1997, **108**, 1.
17. K. L. Yeung, S. T. Yau, A. J. Maira, J. M. Coronado, J. Soria, and P. L. Yue, *J. Catal.*, 2003, **219**, 107.
18. J. C. Yu, J. Yu, W. Ho, and J. Zhao, *J. Photochem. Photobiol. A: Chem.*, 2002, **148**, 331.
19. X. Z. Li, F. B. Li, C. L. Yang, and W. K. Ge, *J. Photochem. Photobiol. A: Chem.*, 2001, **141**, 209.
20. L. Jing, Z. Xu, J. Shang, X. Sun, W. Cai, and H. Guo, *Mater. Sci. Eng. A*, 2002, **332**, 356.

Received December 24, 2005